Activity-dependent production of ATP and ROS in mitochondria of myelinated axons in healthy and neuropathic conditions

Short title: ATP and ROS production in axonal mitochondria

Gerben van Hameren[1]*, Graham Campbell[1], Marie Deck[1], Jade Berthelot[1], Roman Chrast[2], Nicolas Tricaud[1]*

[1] Institut des Neurosciences de Montpellier, INSERM U1051, Université de Montpellier, Montpellier, France

[2] Departments of Neuroscience and Clinical Neuroscience, Karolinska Institutet, Stockholm, Sweden

* Corresponding authors: gerben.van-hameren@inserm.fr

nicolas.tricaud@inserm.fr

Author contributions

GvH conducted the experiments. GvH and NT designed the experiments and wrote the paper with contributions from GC and RC. GC, MD and JB contributed to the experiments and to the design of the experiments. NT supervised the project.

Abstract

Mitochondria are critical for the function and the maintenance of myelinated axons notably through the ATP production. A by-product of this activity is reactive oxygen species (ROS), which are highly deleterious for neurons. While ROS and metabolism are involved in several neurodegenerative diseases, it is still unclear how axonal activity or myelin modulates ATP and ROS production in axonal mitochondria. We imaged and quantified mitochondrial ATP and hydrogen peroxide (H_2O_2) in resting or stimulated peripheral nerve myelinated axons *in vivo*, using genetically-encoded fluorescent probes, two-photon time-lapse and CARS imaging. ATP and H_2O_2 production is intrinsically higher in nodes of Ranvier even in resting conditions. Axonal firing increased both ATP and H_2O_2 productions but with different dynamics. In neuropathic MFN2^{R94Q} mice, mimicking Charcot-Marie-Tooth 2A disease, defective mitochondria failed to upregulate ATP production following axonal activity such as control mice. However, H_2O_2 production was dramatically sustained. Moreover, mimicking demyelinating peripheral neuropathy resulted in a reduced production of ATP while H_2O_2 level soared. Taken together, our results suggest that ATP and ROS productions are decoupled under neuropathic conditions, which may compromise axonal function and integrity.

Keywords: Axons**,** axonal activity, mitochondria, ATP**,** ROS, PNS, demyelination, MFN2.

1. Introduction

While the nervous system, and the brain in particular, represents around 2% of the body mass, it consumes up to 20% of the glucose we mobilize every day [1]. This high energy

expenditure in the nervous system is firstly due to the synaptic activity that requires high amounts of adenosine tri-phosphate (ATP) [1]. A second energy demanding process is the propagation of action potentials (APs) along axons. Indeed, conduction of APs involves ion exchanges through the plasma membrane, first through voltage-gated ion channels to depolarize, then through the sodium-potassium ATPase to repolarize [2,3]. Therefore, the production of ATP in axons is crucial for repeated regeneration of APs. Both in the central nervous system (CNS) and in the peripheral nervous system (PNS), myelination significantly reduces the energy cost of AP propagation through the sequestration of the AP firing machinery at the node of Ranvier and axon initial segment [4].

Mitochondria appear to be the main source of cellular ATP and these organelles are abundant in CNS [5,6] and PNS [7] axons. Some reports indicated that mitochondria were more abundant in the node of Ranvier [8]. In addition, axonal AP activity and axo-glial junctions regulates the recruitment of mitochondria in the nodal area [9]. Therefore, a well-accepted idea is that axonal AP activity could locally stimulate ATP production in axonal mitochondria [10]. However, this nodal enrichment in mitochondria remains controversial [11] and the dynamic of local mitochondrial ATP production following AP is actually unknown.

As an intrinsic by-product of ATP production, mitochondria also produce reactive oxygen species (ROS) [12,13]. The mitochondrial electron transport chain (ETC) and NAPDH oxidases are the major sources of superoxide ($O_2^{\bullet -}$), a highly reactive type of ROS, within cells [14]. $O_2^{\bullet -}$ is rapidly converted to H_2O_2 by superoxide dismutase (SOD) and H_2O_2 is then reduced to H_2O and O_2 by mitochondrial glutathione peroxidase (GPx) and cytosolic enzymes [15]. H_2O_2 can also react with iron or $O_2^{\bullet -}$ to form hydroxyl radicals (OH•), which is then reduced by molecular hydrogen to H_2O [16]. If not reduced by antioxidants, all types of ROS

are highly toxic for the cell and in particular for mitochondria, where they are produced. Indeed ROS can directly oxidize and damage DNA, carbohydrates, proteins or lipids [17].

In several neurodegenerative diseases and axonopathies, such as Parkinson's disease [18], multiple sclerosis (MS) [19] and Charcot-Marie-Tooth diseases (CMT) [20], mitochondrial dysfunction and increased levels of ROS have been shown to be involved. Whether axonal mitochondria are involved is still unclear and investigating the production of ATP and ROS by these mitochondria in active or diseased axons in real time *in vivo* would constitute a first answer.

The importance of mitochondrial homeostasis for the normal function of myelinated axons [9,21] is highlighted by mutations in the *mitofusin 2* (*MFN2*) gene. Indeed, MFN2 has several functions in mitochondria physiology, among which mitochondrial fusion [22] and transport along axons [23], and mutations in its gene result in axonal form of peripheral neuropathy (CMT2A) in humans and in mice [24,25]. In particular, MFN2 loss-of-function in axonal mitochondria decreases the expression of oxidative phosphorylation subunits [26], suggesting that *MFN2* mutations also affect ATP and ROS production. However, this remains to be shown *in vivo*.

MS is a chronic inflammatory disease affecting myelinated tracts in the brain [27]. MS is characterized by demyelinated lesions resulting from the loss of the myelin sheath and the progressive form of MS shows successive events of myelin degeneration and regeneration that damage axons [27]. A common hypothesis is that demyelinated axons are more demanding in ATP in order to maintain their functions and their integrity [28]. Recent data showed that axonal mitochondria complex IV activity is increased in MS lesions and the total

mitochondrial mass is increased [29], suggesting that axonal mitochondria are indeed producing more ATP. In addition, while activated microglia and macrophages are thought to be the initial source of ROS, axonal mitochondria dysfunction and an increase of mitochondrial ROS contribute to progressive MS [30]. Taken together this suggests that the myelin sheath plays a significant role in the maintenance of axonal mitochondria homeostasis and in particular in the production of ATP and ROS in mitochondria.

To answer these questions, we set up an *in vivo* approach using a H_2O_2-sensitive GFP (roGFP-Orp1) [31] and a fluorescent ATP sensor (AT1.03) [32] targeted to mitochondria to image and measure the dynamics of ATP and H_2O_2 production in mitochondria of myelinated axons in myelinated axons of the PNS. Using this approach, we show that both ATP and H_2O_2 levels are increased in mitochondria residing in nodes of Ranvier and that nerve stimulation sharply increases ATP and H_2O_2 production by mitochondria in few minutes. While MFN2 mutations had no effect on basal levels of ATP and H_2O_2 in axons, it prevented the increase of ATP production after nerve stimulation. At the opposite, an increased H_2O_2 production was observed. Moreover, pathological demyelination reduced ATP production while enhancing mitochondrial ROS, showing that both neuropathic conditions decoupled the production of ATP from the production of ROS.

2. Results

2.1. Validation of the mito-roGFP-Orp1 and mito-AT1.03 probes

We used AT1.03, which is a genetically-encoded fluorescence probe based on fluorescence resonance energy transfer (FRET), to detects ATP [32]. This probe consists of the cyan fluorescent protein (CFP) mseCFP, the yellow fluorescent protein (YFP) variant monomeric

Venus, both linked at the ε-subunit of the Bacillus subtilis FoF1-ATP synthase. In the presence of ATP, the ε-subunit retracts to bring the two fluorescent proteins close to each other, thereby increasing FRET efficiency. The conformational change is reversible. Relative ATP levels are measured using the YFP/CFP fluorescence ratio.

Redox sensitive GFPs (roGFPs) harbor an engineered dithiol/disulfide switch on their surface, which determines their wavelength of excitation [33]. RoGFP2 has been converted into an H_2O_2 specific probes by fusion with the microbial H_2O_2 sensor Oxidant Receptor Peroxidase 1 (Orp1) [31]. The reaction is reversible via reduction by cellular thioredoxin (Trx) or GRx/GSH [34]. Relative H_2O_2 levels are measured using the ratio of emitted fluorescence lights when excited at 800nm (oxidized form) or 940nm (reduced form). All experiments were done in the same imaging conditions and analysis. As both probes are ratiometric, the measured values are independent of the number of mitochondria or of the absolute fluorescence intensity of the probe. Both probes were targeted to the mitochondrial matrix.

We first validated mito-roGFP-Orp1 and mito-AT1.03 probes *in vivo*. Injection of AAV9-mito-roGFP-Orp1 and AAV9-mito-AT1.03 in the spinal cord of mouse pups one day after birth (P1) resulted in expression of the fluorescent probes in multiple axons that are part of sciatic and saphenous nerves (Fig 1A). Coherent Anti-stokes Raman Scattering (CARS) microscopy uses the non-linear interactions between light and molecules to generate light from lipids without labeling [35]. As myelin is enriched with lipids, CARS microscopy allows visualizing the myelin sheath around axons *in vivo* [36,37,38]. Using this technique, we observed that the fluorescent probe signal was encompassed by the myelin sheath, which shows the probes are expressed in myelinated axons (Fig 1A). We then performed an immunostaining of teased fibers for the mitochondrial marker TOM20 and observed a partial

colocalisation between fluorescent probes and mitochondria (Fig 1B), showing probes are expressed in axonal mitochondria, but not all of them. Consistently, mitochondria located in Schwann cells surrounding axons were labeled with TOM20 antibody but not with fluorescent probes. Both probes could be detected in axons of the mouse saphenous and sciatic nerves *in vivo*.

Then the ratio of the fluorescent intensity of oxidized/reduced roGFP-Orp1 (R) was followed over time (Fig 1C), showing a small and slow increase of the ratio (0.206 ± 0.002 per hour) probably due to air oxidation. Addition of reducer DTT on the nerve resulted in a significant decrease of the fluorescence ratio, while injection of oxidizer diamide resulted in a significant increase of fluorescence ratio (Fig 1D). These results show that the dithiol/disulfide switch of mito-roGFP-Orp1 is an efficient and reliable indicator of relative redox changes in axonal mitochondria of mouse peripheral nerves *in vivo*. The fluorescence ratio YFP/CFP of mito-AT1.03 (R) was very stable over time (Fig 1E). Injection of 0.4M and 1M ATP into the sciatic nerve in an increase of AT1.03 fluorescence ratio (Fig 1F), showing this probe is also functional *in vivo*.

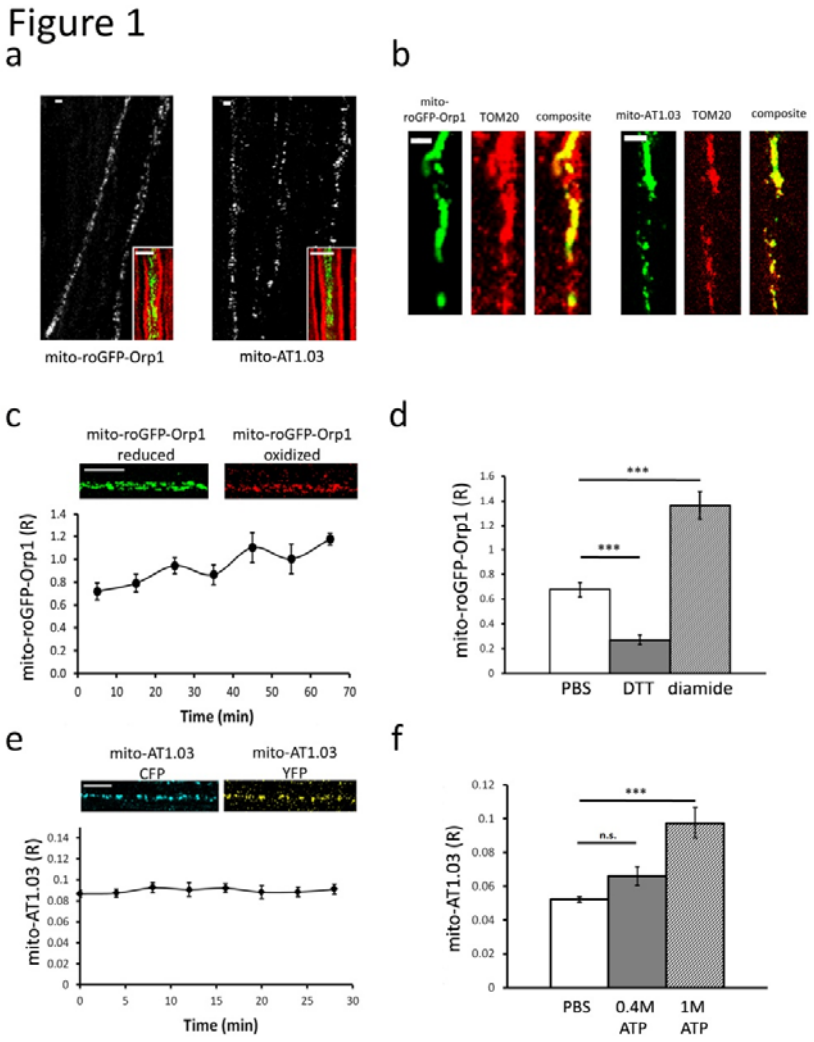

Figure 1: *In vivo* validation of the fluorescent probes.

(A) Several axons expressing mito-roGFP-Orp1 or mito-AT1.03 probe can be observed in teased fibers of mouse sciatic nerve 1 month after the virus injection. CARS imaging (inserts) shows that axons expressing mito-roGFP-Orp1 or mito-AT1.03 (green) are surrounded by a myelin sheath (red). Scale bars = 3 µm. **(**B) mito-roGFP-Orp1 expression (green) partially colocalizes with mitochondrial marker TOM20 (red) in the axon. Similarly, mito-AT1.03 partially colocalizes with TOM20 in axonal mitochondria. Scale bars = 3 µm. (C) A fluorescent signal of mito-roGFP-Orp1 is detected when the probe is reduced and when it is oxidized by H_2O_2. The ratio of mito-roGFP-Orp1 fluorescence measured *in vivo* (n=6 axons; 6 mice) shows a slight increase over time. Scale bar = 10 µm **(**D) Mito-roGFP-Orp1 fluorescence ratio decreases with DTT (p=0.006; n=3 axons, 3 mice) and increases after injection of diamide into the nerve (p=0.003; n=4 axons, 4 mice). (E) A fluorescent signal of the CFP subunit and YFP subunit of mito-AT1.03 is detected. Mito-AT1.03 fluorescence ratio measured *in vivo* shows no significant change over time (n=18 axons; 3 mice). Scale bar = 10 µm. (F) Mito-AT1.03 fluorescence ratio increases after injection of 0.4M (p=0.06; n=3 axons, 3 mice) and 1M (p<0.001; n=6 axons, 4 mice) ATP into the sciatic nerve. All error bars show SEM. Statistical analysis shows Student two-tailed T-tests.

2.2 The effect of nerve stimulation on ATP and H_2O_2 production

While ATP is supposed to be critical for the firing of axons, ATP production in mitochondria of functionally active axons has never been observed *in vivo*. We used the real-time imaging approach previously described in combination with a setup for electrical nerve stimulation based on previous work [39] (Fig 2A-D). We used the saphenous nerve, which is mostly composed of sensory axons, hence its stimulation leads to only limited unwanted contraction of the paw's muscles [40]. After recording the probe fluorescence for at least 20 minutes without stimulation, APs were induced by an electrical burst stimulation protocol including 3 bursts of 50Hz for 30 seconds spaced by a 60 second recovery period (Fig 2E).

Figure 2

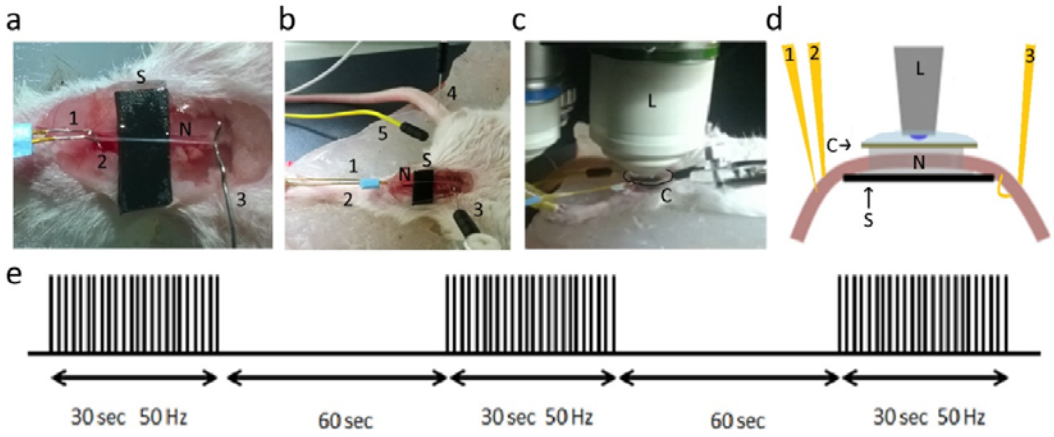

Figure 2: Setup of the saphenous nerve imaging experiment.

(A) After deep anesthesia, the mouse is placed on its back, the skin of its left inner tight is removed and the saphenous nerve (N) is placed on a plastic strip (S). Two stimulation microelectrodes (1 and 2) are inserted on both sides of the nerve on the plastic strip and one hook-shaped recording electrode (3) is holding the nerve on the opposite side. (B) The ground electrode (4) is inserted in the mouse tail and the negative electrode (5) in the groin area. (C) A glass coverslip (Co) is then placed on the nerve soaked in PBS and the mouse is then placed under the two-photon microscope immersion lens 20X (L) in water. (D) Schematic view of the imaging setup. (E) Schematic representation of the nerve stimulation pattern used to induce APs. The generation of APs was verified using the recording electrode. Negative electrode was used to correct for background signal.

The fluorescent signal of mito-AT1.03 was recorded every 5 minutes for 20 minutes after stimulation (Fig 3A). At each time point the fluorescence ratio (R) was corrected for the mean fluorescence ratio of that same axon before nerve stimulation (R0). After a first stimulation, the fluorescence ratio of mito-AT1.03 increased in several axons, but not in all of them (44%), resulting in a slight non-significant average increase (Fig 3a). After the second stimulation, all axons responded significantly increasing mitochondrial ATP production (Fig 3a). In the same conditions, nerve stimulations significantly increased mitochondrial H_2O_2 production just 1 minute after the stimulation period (Fig 3B). H_2O_2 level then quickly went back and stabilized at pre-stimulation values (Fig 3B). These data show that axonal mitochondria very quickly adapt to the axonal activity up-regulating their production of ATP. Spikes in mitochondrial H_2O_2 production were also observed just before the surge of ATP in mitochondria (Fig 3C), suggesting that this H_2O_2 production reflects the oxidative phosphorylation process.

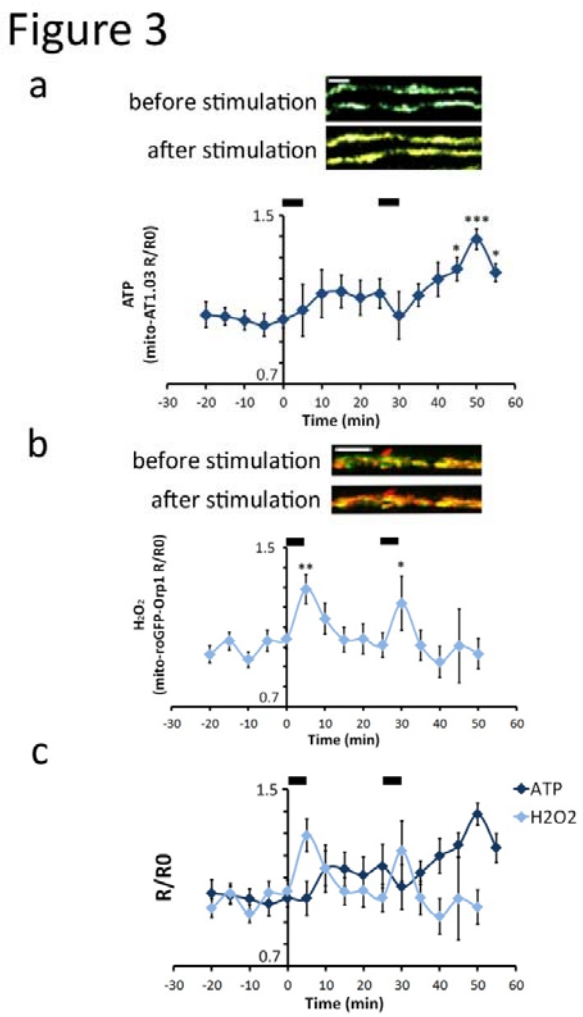

188

Figure 3: Effect of burst nerve stimulation on mitochondrial ATP and H_2O_2 levels.

(A) Upper panels: Nerve stimulation induced changes in the fluorescence signal of both the CFP and YFP subunit of mito-AT1.03 as illustrated by the YFP/CFP overlay pictures. Lower panel: graph showing mito-AT1.03 fluorescence ratio normalized to pre-stimulation values (R/R0) following two successive nerve stimulation period (black bars at the top). The first stimulation results in a slight, non-significant increase; a significant increase is measured after a second stimulation (p=0.0171 at t=45, p=0.0001 at t=50, p=0.049 at t=55; F-value = 2.872; Df=15; n=9 axons in 3 mice). (B) Upper panels: Nerve stimulation induced changes in the fluorescence signal of both the oxidized and reduced forms of GFP in mito-roGFP-Orp1 as illustrated by the overlay pictures. Lower panel: graph showing mito-roGFP-Orp1 fluorescence ratio normalized on pre-stimulation values (R/R0) following two successive nerve stimulation (black bars at the top). Both stimulations result in a significant increase 5 minutes after the stimulation (p=0.007; p=0.04; F-value = 2.804; Df=14; n=14 axons in 7 mice). (C) Graphs described in a and b were overlaid to show the relative dynamics of ATP and ROS levels after nerve stimulations. Scale bars= 5 µm. Error bars show SEM. Statistical tests are one-way ANOVA.

189

2.3. ATP and H_2O_2 production are altered in CMT2A neuropathic mice

We recently showed that MFN2^{R94Q} mice, a model for CMT2A disease [25] where MFN2 is defective, displayed altered mitochondria motility and clustering in peripheral nerve axons [41]. We used this model to measure the level of ATP in axonal mitochondria of myelinated axons in neuropathic conditions. In non-stimulated conditions, control and mutant mice axonal mitochondrial ATP production were similar (Fig 4A). After the first stimulation, similar to control mice, mitochondrial ATP production increased in some axons whereas others did not respond, resulting in statistically non-significant variation (Fig 4B). However, after a second period of nerve stimulation, as opposed to controls, MFN2^{R94Q} axonal mitochondria failed to upregulate ATP production (Fig 4B-C). This indicates that dysfunctional MFN2 does not hinder the basal production of ATP by axonal mitochondria but impairs their ability to up-regulate their production in response to axonal activity.

Similar to ATP, we found no difference between controls and MFN2^{R94Q} mice in the basal H_2O_2 levels (Fig 4D). When nerves were stimulated, mitochondrial H_2O_2 significantly increased after each stimulation period (Fig 4E). However, this increase was delayed compared to controls and H_2O_2 levels remained high for longer time (Fig 4F), showing that axonal mitochondria produce more deleterious H_2O_2 than control mice in response to axonal activity. Since ROS production in the mitochondrial matrix reflects the oxidative phosphorylation process [42,43], these data indicate that oxidative phosphorylation is decoupled from ATP production in mitochondria of these neuropathic mice.

Figure 4

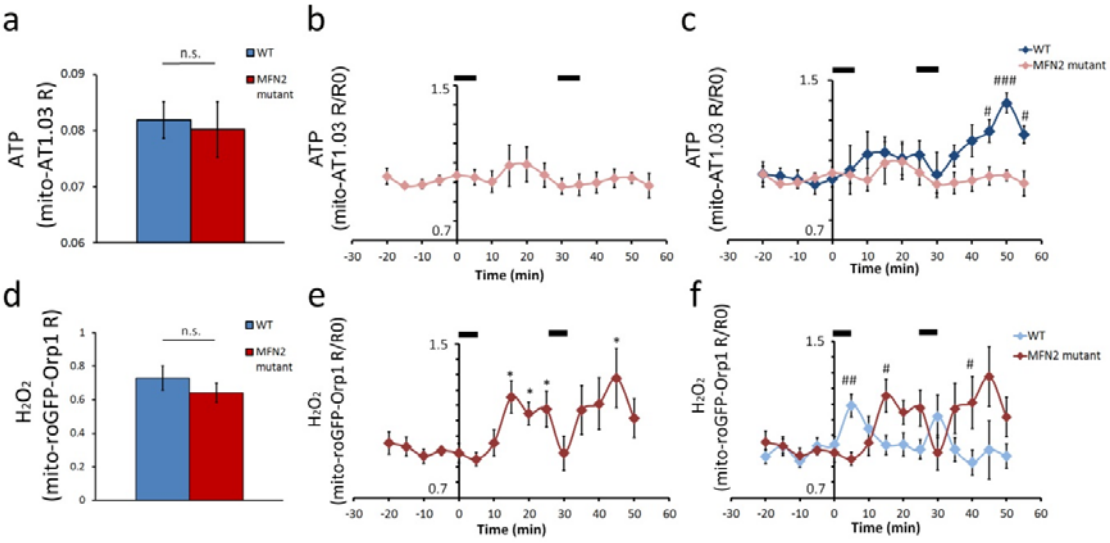

211

Figure 4: ATP and H_2O_2 levels of MFN2^{R94Q} mice.

(A) Graph showing mito-AT1.03 fluorescence ratio in resting axonal mitochondria of wild-type or mutant MFN2^{R94Q} mice (Student two tailed T-test p=0.809; n=18 axons, 7 mice per group). (B) Graph showing mito-AT1.03 fluorescence ratio normalized on pre-stimulation values (R/R0) following two successive nerve stimulation periods (black bars at the top). The first period of stimulation resulted in a slight, non-significant increase; the second stimulation period did not generate any change (n=14 axons in 5 mice). (C) Graphs showing mito-AT1.03 R/R0 in wild-type (Fig. 3A) and mutant MFN2^{R94Q} mice (B panel) were overlaid to show the relative dynamics of ATP levels in both genotypes after nerve stimulations (Two way ANOVA, p=0.011 at t=45, p<0.001 at t=50, p=0.02 at t=55, F-value=19,27; Df=1). (D) Graph showing mito-roGFP-Orp1 fluorescence ratio in resting axonal mitochondria of wild-type or mutant MFN2^{R94Q} mice (Student two tailed T-test p=0.337; n=16 axons, 8 mice per group). (E) Graph showing mito-roGFP-Orp1 fluorescence ratio normalized on pre-stimulation values (R/R0) following two successive nerve stimulation periods (black bars at the top). Both stimulations result in a significant increase (p=0.013 at t=15, p=0.020 at t=20, p=0.044 at t=25 and p=0.038 at t=45; F-value=3.095; Df=14; n=11 axons in 4 mice). (F) Graphs showing mito-roGFP-Orp1 R/R0 in wild-type (Fig. 3B) and mutant MFN2^{R94Q} mice (E panel) were overlaid to show the relative dynamics of H_2O_2 levels in both genotypes after nerve stimulations. A significant higher H_2O_2 level is detected in wild-type first (Two way ANOVA, p=0.007 at t=5, F-value= 5,484; Df=1), then a higher H_2O_2 level is detected in mutant MFN2^{R94Q} (p=0.014 at t=15, p=0.047 at t=40). Error bars show SEM. # = p-value<0.05. ## = p-value<0.01. ### = p-value<0.001.

212

213

214 *2.4. ATP and H2O2 production in nodes of Ranvier and internodes*

215

The enrichment of mitochondria at the node of Ranvier and whether these nodal mitochondria are more metabolically active remains controversial. In order to detect potential spatial differences between nodal and internodal mitochondria, we used CARS microscopy. Gaps in CARS signal between two myelinated internodes are nodes of Ranvier (Fig 5A) [38,43,44]. Combining two-photon imaging of fluorescent probes with CARS imaging allowed us to analyze mitochondrial physiology in nodes of Ranvier versus internodes defined as areas distant of more than 5 µm from the node (Fig 5A). In all observed nodes of Ranvier, probes-labeled mitochondria were present, but they were not more abundant or larger than in internodes (Fig 5A). However, when measuring the mito-AT1.03 and mito-roGFP-Orp1 fluorescence ratio, we found significantly higher ATP and H_2O_2 levels in node of Ranvier mitochondria (Fig 5B-C). These data, obtained in resting animal without nerve stimulations, indicate that nodal mitochondria are intrinsically more metabolically active than internodal ones. In neuropathic $MFN2^{R94Q}$ mice, nodal mitochondria did not show a higher level of ATP versus internodal mitochondria (Fig 5B). However, they still had higher level of H_2O_2 (Fig 5C), suggesting again a decoupling between oxidative phosphorylation and the production of ATP in mitochondria of these mutant mice.

Figure 5

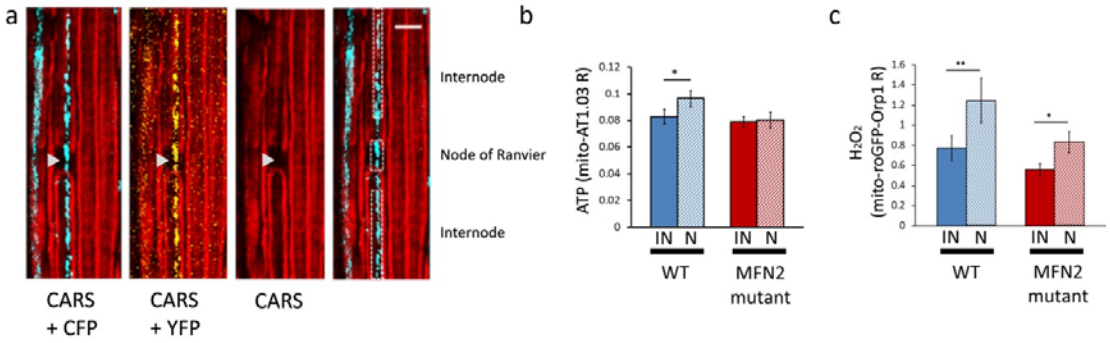

Figure 5: ATP and H_2O_2 levels are different along axons.

(A) Two-photons imaging of CFP (blue) and YFP (yellow) fluorescence of mito-AT1.03 was combined with CARS imaging of the myelin sheath (red). CARS imaging gap shows a node of Ranvier (arrowhead). Using the combined images, mitochondria located in the node of Ranvier and mitochondria located in internodes can be identified (right panel). Scale bar = 10 µm (B) Graph showing mito-AT1.03 fluorescence ratio in axonal mitochondria located in nodes of Ranvier (N) or internodes (IN) of wild-type (WT) or $MFN2^{R94Q}$ mice (MFN2 mutant). In wild-type mice, ATP levels are higher in mitochondria in nodes of Ranvier than in internodes (p=0.035; n=14 axons in 7 mice). In $MFN2^{R94Q}$ mice, ATP levels in node of Ranvier mitochondria are equal to internode mitochondria (n=7 nodes in 3 mice). (C) Graph showing mito-roGFP-Orp1 fluorescence ratio in axonal mitochondria located in nodes of Ranvier or internodes of wild-type or mutant $MFN2^{R94Q}$ mice. In both wild-type mice and mutant $MFN2^{R94Q}$ mice, H_2O_2 levels are higher in mitochondria in nodes of Ranvier than in internodes (WT: p=0.009; n=8 axons in 3 mice. $MFN2^{R94Q}$: p=0.019; n=9 axons in 3 mice). Error bars show SEM. Statistical tests are Paired T-tests.

2.5. ATP and H_2O_2 production in mitochondria of demyelinated axons

The myelin sheath is critical to maintain the node of Ranvier on myelinated axons and is therefore likely to play a significant role in the homeostasis of axonal mitochondria. As demonstrated in Fig 5a, the myelination state of the axons in the mouse sciatic nerve can be assessed *in vivo* by CARS imaging. We therefore investigated how this demyelination affects axonal mitochondria physiology *in vivo*. To induce demyelination we used lyso-phosphatidylcholine (LPC) and we followed the production of mitochondrial ATP and H_2O_2 in axons during demyelination and during the restoration of the myelin sheath

(remyelination). LPC, which is a signaling molecule resulting from the hydrolysis of phophatidylcholine by phospholipase A2 [45] acts in mSC and oligodendrocytes as a demyelinating signal [46,47,48]. LPC was injected in the sciatic nerve of adult mice and demyelination occurred immediately to culminate one week after the injection with the formation of myelin ovoids and debris as seen using CARS (Fig 6A, week 1) [37,49]. As soon as two weeks after LPC injection, remyelination occurred and some thin myelin sheaths reappeared around axons (Fig 6A, week 2). Axons were completely remyelinated three weeks after injection of LPC (Fig 6a, week 3). No demyelination occurred in control mice injected with PBS (Fig 6A last panel). Axonal integrity is not directly affected by LPC (S1 Figure) [50] and axonal mitochondria remained visible using either mito-AT1.03 or mito-roGFP-Orp1 probes during the entire process of demyelination and remyelination (Fig 6A inserts).

Figure 6

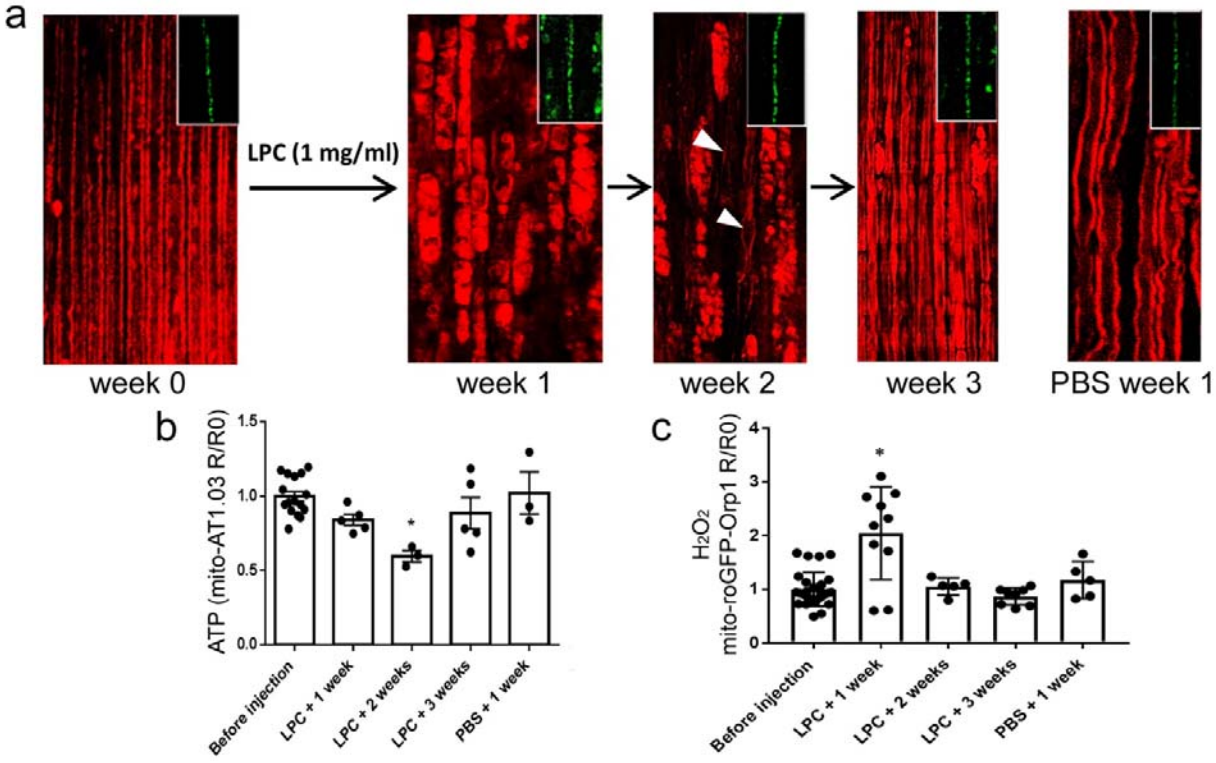

Figure 6: Impact of demyelination on axonal mitochondria ATP and H_2O_2.

(A) CARS imaging is used to visualize myelin. At week 0, before injection of LPC, most axons are myelinated. 1 week after LPC injection, axons are demyelinated and myelin debris and ovoids are observed. At week 2, thinly myelinated axons are observed in between the myelin debris (arrowheads) and at week 3, almost all axons are myelinated again, thus resembling a healthy nerve. PBS injection induces small conformational changes, but no formation of ovoids or debris. Inserts show that neuronal mitochondria remain visible throughout the whole process. (B) Graph showing mito-AT1.03 fluorescence ratio (R) in axonal mitochondria normalized on pre-demyelination values (R0) following demyelination. Following LPC injection, ATP levels are unchanged after 1 week (p=0.085; n=5 mice; 27 axons), decreased after 2 weeks (p=0.019; n=3 mice, 24 axons) and restored after 3 weeks (p=0.491; n=5 mice; 31 axons). PBS injection results in no significant change (p=0.799; n=3 mice; 23 axons). (C) Graph showing mito-roGFP-Orp1 fluorescence ratio (R) in axonal mitochondria normalized on pre-demyelination values (R0) following demyelination. Following LPC injection, H_2O_2 levels are increased after 1 week (p=0.031; n=10 mice, 17 axons), and unchanged after 2 weeks (p=0.663; n=5 mice, 9 axons) and after 3 weeks (p=0.450; n=8 mice, 13 axons). PBS injection results in no significant change (p=0.121; n=3 mice, 5 axons).

We therefore measured the fluorescence ratio for these probes in non-stimulated axonal mitochondria during the process. One week after LPC injection, when axons are completely demyelinated, ATP production was slightly lower than before demyelination, but not significantly (Fig 6B), while H_2O_2 levels peaked (Fig 6C). ATP levels were significantly lower in axonal mitochondria at two weeks after LPC injection, while H_2O_2 levels were back to control and pre-demyelination levels (Fig 6B-C). Finally, three weeks after injection, when remyelination is completed, ATP levels were back to control and pre-demyelination levels as are the H_2O_2 levels (Fig 6B-C). No change either in ATP or H_2O_2 levels were detected at one week after injection with PBS in control mice (Fig 6B-C). Moreover, increase in ROS did not result from a general oxidative stress in the demyelinated nerve, since CellRox dye did not show any significant increase, except at the LPC injection site where we did not image our probe (S1 Fig). Taken together, these data indicate that the myelin sheath has a profound impact on axonal mitochondria physiology. Mitochondria manage to maintain their ATP production during myelin break-down, but they generate more H_2O_2. The process of

remyelination leads to decreased production of ROS, while ATP production is temporally diminished before full remyelination. These data therefore indicate that demyelination induces the decoupling of ATP production from oxidative phosphorylation.

3. Discussion

Although it has been shown that PNS axonal mitochondria, like most mitochondria, produce both ATP and ROS, the regulations of their production are still not well understood *in vivo* and *in situ*. We used a combination of viral delivery of mitochondria-targeted fluorescent probes to active peripheral neurons and two-photon and CARS live imaging in mice to fill that gap. The mito-AT1.03 and mito-roGFP-Orp1 fluorescent probes had been previously validated *in vitro* [51] and *in vivo* [33] in other systems but we also validated them *in vivo* in our system. We did not attempt to measure absolute values of ATP or H_2O_2 with each probe fluorescence *in vivo* because firstly, this was difficult as probes are targeted to mitochondrial matrix and secondly, it was not necessary as we aimed to compare different genotypes and conditions in particular with time. So only relative values obtained in the same imaging conditions are shown here. We found that the range of detection was large enough to cover the changes occurring in axonal mitochondria *in vivo*. Moreover the probe sensitivity was sufficient to observe variations in real-time using a 5 minutes delay between measures. This delay was partly imposed by relative low speed of our imaging system (1 minute to create 10 scans of 200µm^2 over 40 µm depth for each wavelength), but also by the intrinsic limits of our set-up: electrical stimulation induced slight contractions of saphenous nerve surrounding muscles which made the pictures blurred during the stimulation. The probes alterations were also reversible fast enough to observe changes in both directions. Mito-AT1.03 was stable, but mito-roGFP-Orp1 showed a slight increase of its fluorescence ratio over time under our

296 experimental settings. These results are not explained by photobleaching or degradation of the
297 probe, since the total fluorescent signal does not decrease. This change in ratio of
298 fluorescence may be caused by air oxidation [52]. However, buffered artificial cerebrospinal
299 fluid as an incubation medium for the saphenous nerve did not prevent the probe oxidation.
300 Nonetheless, this slow oxidation of mito-roGFP-Orp1 had negligible effects on our
301 experiments, since it was too slow to cause significant changes in our relatively short term
302 imaging.
303
304 Axonal activity induced stereotypic changes in ATP and H_2O_2 production by axonal
305 mitochondria. Shortly after the stimulation, H_2O_2 production increased and dropped
306 immediately and then ATP increased for several minutes. This was stereotypic, because it
307 occurred almost identically after both stimulations we did. After the first stimulation, not all
308 axonal mitochondria produced more ATP, suggesting that either our stimulation protocol was
309 not mobilizing enough axons or axonal mitochondria are deactivated, similar to some ion
310 channels. This limitation was lifted by the second stimulation. On the attempts we did for
311 further stimulations, sometimes the ATP level was maintained at high range and sometimes
312 mitochondria did not respond anymore. The reason for these variations in the long term is
313 unknown and we did not pursue this further. However, taken together, this suggests that ATP
314 production in axonal mitochondria is positively correlated with the level of axonal activity
315 and can eventually reach a plateau in our conditions. Due to technical reasons we could not
316 measure H_2O_2 levels in mitochondria after several stimulations. However, looking at the first
317 two stimulations, we conclude that H_2O_2 production in mitochondria is also positively
318 correlated with axonal activity but not cumulative. It would be interesting to look further for
319 the molecular mechanisms that allow mitochondria to detect axolemma depolarization or ion
320 channels activity on a very short period of time (around one minute in our detection

capacities). This fast kinetic suggests the role of ions, such as calcium ions, which are mobilized during AP firing at the node of Ranvier [53], or kinases. A mechanism involving calcium has been shown to anchor mitochondria at the node of Ranvier [54], suggesting that mitochondria are associated with the axolemma there. Consistently, we found nodal mitochondria to be more metabolically active than internodal ones. However, our data following stimulations were recorded on mitochondria independently of their location on axons. As the node is much smaller than the internodes (1 µm versus 600 µm in average in the mouse nerve) the probability we recorded nodal mitochondria is extremely small. So the molecular mechanism that mobilizes mitochondria after AP firing has to exist also in internodal mitochondria.

Looking at the known origin of ROS in mitochondria, our data suggest that the H_2O_2 production we detected in axonal mitochondria reflects the loading of the mitochondrial matrix with protons before the production of ATP. However, since the H_2O_2 production drops very quickly and, contrary to the ATP production, it is not cumulative, a more complex scheme has to be taken in consideration. Indeed, H_2O_2 is formed by SOD enzyme from $O_2^{\bullet -}$, which directly results from the ETC. Moreover, H_2O_2 is then changed in H_2O and O_2 by several reducing enzymes, such as mitochondrial GPx, so actually the amount of H_2O_2 we detected is the result of equilibrium between $O_2^{\bullet -}$ production and SOD and reducing enzymes' activities. As these enzymes are highly expressed in mitochondria [55], they probably do not constitute a limiting factor and the H_2O_2 levels we detected still reflect axonal mitochondria metabolic activation. However, H_2O_2 levels drop quickly, probably because reducing enzymes are removing it quickly. In addition, these enzymes' activities change following fast post-translational modifications such as phosphorylation [56] or environmental changes [57].

345 While this may explain why H_2O_2 levels are not incremental following several stimulations,
346 further investigation will be needed to clarify underlying mechanisms.
347
348 Several CNS and PNS neuropathies are linked to mitochondrial dysfunctions in neurons
349 [18,19,20]. Our data show that the electrical activity of neurons directly regulates the
350 physiology and the respiration of axonal mitochondria. As axonal mitochondria are the most
351 abundant among neuronal mitochondria, this suggests that axonal mitochondria dysfunctions
352 may severely impact neuronal physiology and survival. We evaluated this hypothesis using a
353 couple of peripheral neuropathy mouse model, such as a model of CMT2A disease expressing
354 mutant $MFN2^{R94Q}$ [25]. While *in vitro* data had shown increased H_2O_2 levels [58], but no
355 change in ATP production [59] in neuronal mitochondria of these mice, *in vivo* we did not
356 measure significant differences in these parameters between resting $MFN2^{R94Q}$ mice and
357 control mice. A first explanation for this discrepancy is that cultured cells are living in an
358 environment that is significantly different from the *in vivo* conditions. This is especially true
359 in terms of metabolism [60]. Another explanation is that mitochondria physiology is altered,
360 but this can only be seen when mitochondria are challenged. Environmental changes in
361 culture may constitute this challenge, while more physiologically relevant challenges have to
362 be found *in vivo*. Our electrical stimulations were physiologically meaningful challenges for
363 axons and, similar to control mice, we observed ATP levels increasing in several axons of
364 mutant mice, but not all, after a first nerve stimulation. However, while control mice
365 mitochondria increased their ATP production further following a second stimulation, no
366 increase was observed in mutant mice mitochondria. We have shown that Mitochondria
367 Associated Membranes (MAM), which mediate interactions between the endoplasmic
368 reticulum and mitochondria [41], are impaired in these mutant mice. So we suggest that an
369 impaired Ca^{2+} uptake by mitochondria through MAM [61] could alter the ATP production as

370 it has been shown that calcium is required for the TCA cycle [62]. However, mutant mice
371 mitochondria were still able to produce a large amount of H_2O_2 following both stimulations,
372 suggesting the ETC and therefore the TCA cycle are working properly. Yet this H_2O_2
373 production was completely abnormal: it was largely delayed and was sustained for over at
374 least 10 minutes. As discussed before the levels of H_2O_2 result from an equilibrium between
375 several parameters, so it is difficult to explain this abnormal production. Nevertheless, a
376 relationship between mitochondrial shape and ROS has been shown *in vitro* [63]. It has been
377 suggested that smaller mitochondria result in intra-mitochondrial redistribution of cytochrome
378 c and the pro-aging molecule p66shc that acts trough ROS upregulation [64,65]. Smaller
379 fragmented mitochondria, such as MFN2 mutants [63], correlate with a malfunctioning
380 antioxidant system and an increased production of ROS [58,64]. In any case, our data show
381 that an altered MFN2 function lead to the dysfunction of axonal mitochondria only when
382 axons are firing. This dysfunction is strongly deleterious as mitochondria don't produce more
383 ATP but show a sustained production of deleterious ROS. This functional decoupling between
384 ATP and H_2O_2 production, occurring in the most abundant mitochondria of the neurons and in
385 conditions of normal firing activity, is likely to be a significant cause of the neuronal
386 dysfunction in this peripheral neuropathy.
387
388 Looking at the node of Ranvier of MFN2 mutant mice, we found that, similar to control mice,
389 nodal mitochondria were more metabolically active than internodal ones. As MFN2 mutant
390 mitochondria do not increase ATP production in active axons, this suggests that nodal
391 mitochondria are intrinsically more active even in absence of firing. This is consistent with
392 the fact that motile mitochondria slow down in the nodes of Ranvier [6] and that they have a
393 different morphology [66]. Moreover, nodal mitochondria may participate to axonal
394 degeneration since this process starts in nodes of Ranvier due to high ROS levels [67]. It

would have been interesting to investigate changes occurring in ATP and H_2O_2 production of nodal mitochondria after electrical stimulation but this was impossible due to the small size of the node and the change of focus that occurs following stimulations.

The myelin sheath that covers axons appears to be an important regulator of axonal metabolism and of mitochondria physiology. Indeed in MS, demyelination alters axonal mitochondria [19,29,68] and we show here that nodes of Ranvier devoid of myelin house more metabolically active mitochondria. To go further, we therefore investigated the impact of the loss of myelin on axonal mitochondria. LPC was the right tool because it induced demyelination without destroying axons [46,47,48]. LPC-induced demyelination resulted in a decrease of ATP levels in axonal mitochondria. This decrease was strongest after two weeks and was reversed by 3 weeks, showing that ATP production within neurons is impaired until complete remyelination. This decrease was unexpected, since AP propagation in demyelinated axons is more energy demanding: the nodal machinery and the Na^+/K^+ ATPase are diffused all along the axolemma and all the energy-effective benefits of myelination are lost [69]. In demyelinated area of brains affected by MS, an upregulation of ETC complexes protein expression and more complexes I and IV activity [68] was observed. Moreover, demyelinated axons showed more mitochondria [29], which is consistent with a higher energy demand.

Nevertheless, H_2O_2 levels strongly increased in axonal mitochondria of fully demyelinated axons in absence of general oxidative stress in the tissue. This decoupling of mitochondrial oxidative phosphorylation and ATP production is in accordance with previous studies that reported a decreased ATP production, together with increased ROS levels in demyelinating diseases [70]. This suggests that actually, mitochondrial ETC complexes are more active and

produce more ROS, but this does not lead to more ATP production. Such a mechanism has been shown in particular conditions where the goal of mitochondrial activity is to produce heat. Uncoupling proteins such as UCP2 permeabilize the inner mitochondrial membrane to dissipate the proton gradient [71]. This may not be the sole utility of uncoupling as this process has been shown to occur in several neurodegenerative diseases [72]. However, so far we failed to detect unusual UCP2 expression in demyelinated nerves. The high production of H_2O_2 during demyelination is probably not without consequences as ROS can alter the function of the ATP synthase [73]. This may explain why ATP production remains weak in mitochondria of axons that are being remyelinated two weeks after LPC injection, despite that ROS production is back to normal. This suggests that during demyelination, axons may recruit more mitochondria [29], or use another metabolism, such as aerobic glycolysis, in order to cover their need in ATP.

While very little amount of data exists on the homeostasis of axonal mitochondria in demyelinated axons of the PNS, in the CNS, demyelination in progressive MS results in axonal mitochondria dysfunction and ROS increase [74]. The data we collected in PNS myelinated axons on ROS production by axonal mitochondria are consistent with this. This suggests that, despite the large difference that exists between PNS and CNS myelinating glia, their similar role in segregating axonal firing machinery at nodes of Ranvier is essential for mitochondria homeostasis in axons. Nevertheless, the electrical isolation of the axon and the formation of the node of Ranvier is not the only function of the myelin sheath as it also largely participates to the metabolic homeostasis of the axon through the lactate shuttle process [75,76]. This is particularly true for the CNS myelin [76]. In addition, MS disease is significantly different from peripheral nerve diseases, in particular because of the important role played by CNS glial cells astrocytes and microglia. So, it would be essential to confirm

445 the data we obtained in PNS myelinated axons in CNS myelinated axons *in vivo*, in order to
446 definitely conclude on the alteration of ATP and ROS production by axonal mitochondria in
447 demyelinated lesion of progressive MS.
448
449 To conclude, combining several novel techniques such as two-photon and CARS non-linear
450 live imaging coupled to electrical nerve stimulation and genetically-encoded fluorescent
451 probes delivered by AAV vectors, we were able to observe the production of ATP and H_2O_2
452 by axonal mitochondria in real time and in living and active axons of mouse peripheral
453 nerves. We demonstrated that mitochondria are more metabolically active at the node of
454 Ranvier and we characterized the role of AP firing in the dynamics of mitochondrial ATP and
455 H_2O_2 production. Moreover we show the deleterious alterations that occur in axonal
456 mitochondria physiology of two mouse models of neuropathy, peripheral axonal CMT2A and
457 demyelinating peripheral neuropathies. Together, our data thus provide new insight into the
458 role of axonal mitochondria under physiological and pathological conditions.
459
460 **4. Materials and methods**
461
462 *4.1. Cloning*
463
464 pLPCX mito-roGFP-Orp1 (Addgene; #64992) was digested with XhoI/ClaI, blunted and
465 cloned into pAAV-MCS (Cell Biolabs, Inc.) under the control of a CMV promoter. Clones
466 were validated by sequencing. Likewise, pcDNA-mito-AT1.03 (from H. Imamura, Tokyo,
467 Japan) was digested with XhoI/HindIII, blunted and cloned into the CMV promoter controlled
468 pAAV-MCS. Mitochondria-targeting tags were CoxVIII for roGFP-Orp1 and two tandem
469 copies of CoxVIII for mito-AT1.03. AAV viral particles were produced at the viral vector

production centre at the Centre de Biotecnologia Animal I Teràpia Gènica in Barcelona, Spain or the University of Nantes, France.

4.2. Mouse strains

Either Swiss mice (Janvier, France) or MFN2^{R94Q} mice [25] were used in the performed experiments. Mice were kept in the animal facility of the Institute for Neurosciences of Montpellier in clear plastic boxes and subjected to standard light cycles. All animal experiments were conducted in accordance with the French Institutional and National Regulation CEEA-LR-11032.

4.3. In vivo virus injection in spinal cord

A thin borosilicate glass capillary (Harvard Apparatus, Ref. 30-0016) was pulled with a Vertical Micropipette Puller (Sutter Instruments, P30-682) to form a glass needle. The glass needle was filled with viral solution (1 µl) and a 1 day old mouse is restrained in a position that exposes the lower back. The needle is injected through the skin using a micromanipulator and introduced into the spinal cord. The viral solution was injected over 2 minutes with short pressure pulses using a Picopump (World Precision Instrument) coupled to a pulse generator. After injection, the injection site is cleaned with betadine solution (Vetoquinol, cat. no. 3042413) for disinfection and the pup is placed back with its mother and littermates.

4.4. Immunohistochemistry

494 One month after the viral injection, the sciatic nerve was dissected and fixed in Zamboni's
495 fixative [77] for 10 min at room temperature. After fixation, the dissected sciatic nerves are
496 washed in PBS and incubated in successive glycerol baths (15, 45, 60, 66% in PBS) for 18 to
497 24 h each before freezing at −20 °C. The nerves were cut in small pieces in 66% glycerol and
498 the epineurium sheaths removed. Small bundles of fibers were teased in double-distilled water
499 on Superfrost slides and dried for 3 hours at room temperature. Some nerves were frozen in
500 O.C.T. Compound (Tissue-Tek, Ref. 4583) and longitudinal sections were cut using a cryostat
501 (Leica Biosystems, CM3050). For immunostaining, the teased fibers or longitudinal sections
502 were incubated for 1 h at room temperature in blocking solution (10% goat serum and 0.3%
503 TritonX100 in PBS). Then, the samples were incubated with TOM20 (FL-145) primary rabbit
504 antibody (1/500, Santa Cruz, Ref. sc-11415), mouse anti-Myelin Basic Protein (1/500, Merck,
505 Ref. NE1019) or rabbit NF-200 (1/500, Sigma, Ref. N4142) in blocking solution overnight at
506 4 °C. The next day, the samples were washed in PBS and incubated for 1h at room
507 temperature with secondary donkey antibodies coupled to Alexa568 (1/1000, Invitrogen, Ref.
508 A10042) or Alexa488 (1/1000, Invitrogen, Ref. A21202). Finally the samples were washed in
509 PBS and mounted in Immu-mount (Thermo Scientific). Images were acquired at room
510 temperature using a 20× or 40× objective, a Zeiss confocal microscope LSM710, and its
511 associated software.
512
513 *4.5. Imaging of sciatic nerve in living mice*
514
515 One month after the viral injection, the mice were anesthetized with a constant flow (1.5
516 l/min) of oxygen + 5% of isoflurane in an anesthesia box (World Precision Instruments, Ref.
517 EZ-B800) for 5 min. Thereafter the anesthesia was maintained with a mask delivering 2%
518 isoflurane at 0.8 l/min. The eyes were protected by eye protection gel (Ocry-gel, TVM, cat.

519 no. 48026T613/3). Intraperitoneal injection of 0.1 mg/kg buprenorphine was used for pre-
520 surgery analgesia. The mouse was placed in a silicone mold, lying on its belly, shaved on his
521 hind paw and the paws immobilized using small pins. The incision area was disinfected with
522 betadine solution (Vetoquinol, cat. no. 3042413). The skin was cut using scissors, fat tissue
523 removed, the gluteus superficialis and biceps femoris muscles were separated to reveal a
524 cavity crossed by the sciatic nerve, and the sciatic nerve was lifted up using a small spatula. A
525 long plastic strip was placed underneath the sciatic nerve and this strip fixed using magnets.
526 The sciatic nerve was kept in an aqueous environment of either sterile PBS buffer or artificial
527 cerebrospinal fluid (148 mM NaCl, 3 mM KCl, 1.4 mM $CaCl_2$•$2H_2O$, 0.8 mM $MgCl_2$•$6H_2O$,
528 0.2 mM $NaPO_4$•H_2O in sterile H_2O) to prevent drying. At that point the mouse was placed
529 under the two-photon microscope objective lens, a glass, 12mm diameter, 0.25mm thick
530 microscope coverslip put on top of the nerve and a drop of deionized water placed on it to
531 immerse the objective lens (20X, Carl Zeiss Microscopy, LD CApochromat, Ref. 421887–
532 9970).
533
534 *4.6. Demyelination procedure*
535
536 After imaging of the sciatic nerve in vivo for at least 30 minutes, 5 µl of 1 mg/ml
537 lysophotphatidyl choline (LPC) was injected directly into the sciatic nerve using a Hamilton
538 syringe (Ref. 80930) to induce demyelination. Injection of 5 µl PBS is used as a negative
539 control. After injection, the nerve was placed back to its original location in the body. The
540 skin of the incision was realigned together using a blunt scalpel and stapled along the wound
541 with two clips (Fine Science Tools; 12020-00). The area around the wound was disinfected
542 again with betadine solution. The anesthesia mask was removed and the mouse was
543 monitored until it had woken up. Motor function of the injected and non-injected hindlimb

544 was followed by lifting the animal by the tail. At 1 week after LPC injection, the non-injected
545 hindlimb showed a normal postural reflex characterized by spreading of leg whereas the
546 injected hindlimb showed abnormal reflexes such as tremors, clasping or retracting of the
547 paw. This behavior has been described and linked to deficient myelination in the PNS in
548 previous studies [78]. The severity of abnormal hindlimb function decreased at 2 weeks after
549 LPC injection and no difference in leg function between the injected and non-injected
550 hindlimb could be observed anymore at 3 weeks after LPC injection.
551
552 *4.7. Saphenous nerve stimulation in living mice*
553
554 After skin incision and removal of connecting tissue, the saphenous nerve is lifted up and
555 isolated using a plastic strip (Fig 2a). To stimulate the saphenous nerve, two platinum kapton
556 microelectrodes (World Precision Instruments, PTM23B05KT) were inserted at the posterior
557 side of the plastic strip using a micromanipulator (Fig 2A). One hook-shaped recording
558 electrode (AD Instruments, MLA 1203) was placed at the anterior side (Fig 2A). The ground
559 electrode was inserted in the tail of the mouse and the negative electrode in the groin area (Fig
560 2B). The mouse was placed under the two-photon microscope (Fig 2C), a microscope glass
561 coverslip was placed on top of the nerve and the electrodes were connected to a Powerlab 26T
562 (AD Instruments; ML4856). A drop of deionized water was then placed on top of the
563 microscope glass to immerse the 20× objective lens.
564
565 *4.8. Two-photon image acquisition*
566
567 All in vivo images were obtained with a two-photon microscope LSM 7 MP OPO (Zeiss,
568 France) coupled to a dark microscope incubator (L S1 Dark, Zeiss) in which the temperature

569 was maintained at 37 °C (Heating Unit XL S, Zeiss, France). Mitochondria images were
570 acquired by time-lapse recording varying from one image every minute to one image every 5
571 minutes during 1 hour. Each image is a stack at Maximum Intensity (ZEN software, Zeiss) of
572 10 scans over 40 μm depth. For AT1.03 imaging, a single track at 850 nm excitation
573 wavelength is used to obtain both the CFP (em. 475 nm) and YFP (em. 527 nm) image at the
574 same time point. For roGFP imaging, the two images were acquired for each time point using
575 alternating tracks at 940nm and 800nm. Change of track was set after each stack. For
576 Coherent Anti-Stokes Raman Scattering (CARS) imaging, 2 synchronized laser lines at
577 excitation wavelengths 836 nm and 1097 nm are used simultaneously thanks to the OPO
578 system. Each scan was acquired with constant laser intensity (20% for 940 nm, 10% for 850
579 nm, 10% for 800nm, 15% for 836nm, 4% 1097nm) at a 512 × 512 pixel resolution and
580 microscope imaging parameters were maintained over all different regions we imaged.
581 Images, acquired with ZEN software (Zeiss), were saved in .czi format.
582
583 *4.9. Data and statistical analysis*
584
585 We used ImageJ software to analyze the relative ATP or H_2O_2 levels in mitochondria of
586 peripheral axons. The acquired images for each wavelength were aligned using the Template
587 Matching plugin. We defined a Region of Interest (ROI) encompassing all labeled
588 mitochondria of the same axon and the mean fluorescent intensity on the ROI was measured
589 on both images. These light intensities were then corrected for background light intensity
590 determined as an area within the nerve where no fluorescent signal from the viral probe can
591 be observed. Either the AT1.03 YFP/CFP ratio or the oxidized roGFP/reduced roGFP ratio
592 was then calculated from the 2 values for mean light intensity.
593

Statistical significance for the effect of time on probe stability was determined using linear regression. The effects of the positive controls and negative controls on probe validation were determined using Student two-tailed T-tests. The effect of nerve stimulation was determined using one-way ANOVA and Dunnett's post-hoc tests. In addition, the threshold for a responding axon was set at 20% change in probe fluorescence ratio. The differences between MFN2 mutants and wild-type mice were determined using either Student two-tailed T-tests or two- way ANOVA with Sidak post-hoc tests. Differences between internodes and node of Ranvier mitochondria were determined using paired two-tailed T-tests. The effect of demyelination was determined using paired two-tailed T-tests.

4.10. Data and statistical analysis

The data that support the findings of this study are available from the corresponding author upon reasonable request.

5. Financial disclosure

This work has benefited from support by an ERC consolidator grant to NT and by the Labex EpiGenMed ANR-10-LABX-12-01.

6. Acknowledgements

In addition we thank the MRI imaging platform, supported by the French National Research Agency (ANR-10-INBS-04), in particular Hassan Boukhaddaoui, and the Animal Facility of

the INM. We also would like to thank Patrice Quintana for his help with the nerve stimulation protocol and Volker Baeker for the image analysis protocol.

7. Competing interests

The authors declare that the research was conducted in the absence of any commercial or financial relationships that could be construed as a potential conflict of interest.

8. References

1. Harris JJ, Jolivet R, Attwell D. Synaptic Energy Use and Supply. Neuron. 2012 Sep 6;75(5):762–77.

2. Attwell D, Laughlin SB. An Energy Budget for Signaling in the Grey Matter of the Brain. J Cereb Blood Flow Metab. 2001 Oct 1;21(10):1133–45.

3. Ames A. CNS energy metabolism as related to function. Brain Res Rev. 2000 Nov 1;34(1):42–68.

4. Salzer JL, Zalc B. Myelination. Curr Biol. 2016 Oct 24;26(20):R971–5.

5. Fischer TD, Dash PK, Liu J, Waxham MN. Morphology of mitochondria in spatially restricted axons revealed by cryo-electron tomography. PLOS Biol. 2018 Sep 17;16(9):e2006169.

6. Misgeld T, Kerschensteiner M, Bareyre FM, Burgess RW, Lichtman JW. Imaging axonal transport of mitochondria in vivo. Nat Methods. 2007 Jun 10;4:559.

7. Zhou B, Yu P, Lin M-Y, Sun T, Chen Y, Sheng Z-H. Facilitation of axon regeneration by enhancing mitochondrial transport and rescuing energy deficits. J Cell Biol. 2016;214(1):103–119.

8. Ohno N, Kidd GJ, Mahad D, Kiryu-Seo S, Avishai A, Komuro H, et al. Myelination and axonal electrical activity modulate the distribution and motility of mitochondria at CNS nodes of Ranvier. J Neurosci Off J Soc Neurosci. 2011 May 18;31(20):7249–58.

9. Perkins GA, Ellisman MH. Mitochondrial Configurations in Peripheral Nerve Suggest Differential ATP Production. J Struct Biol. 2011 Jan;173(1):117–27.

10. Tarasov AI, Griffiths EJ, Rutter GA. Regulation of ATP production by mitochondrial Ca(2+). Cell Calcium. 2012 Jul;52(1):28–35.

11. Edgar JM, McCulloch MC, Thomson CE, Griffiths IR. Distribution of mitochondria along small-diameter myelinated central nervous system axons. J Neurosci Res. 2008;86(10):2250–7.

12. Giorgio M, Trinei M, Migliaccio E, Pelicci PG. Hydrogen peroxide: a metabolic by-product or a common mediator of ageing signals? Nat Rev Mol Cell Biol. 2007 Sep 1;8:722.

13. Murphy MP. How mitochondria produce reactive oxygen species. Biochem J. 2009 Jan 1;417(Pt 1):1–13.

14. Hamanaka RB, Chandel NS. Mitochondrial reactive oxygen species regulate cellular signaling and dictate biological outcomes. Trends Biochem Sci. 2010 Sep;35(9):505–13.

15. Tormos KV, Chandel NS. Seeing the Light: Probing ROS In Vivo Using Redox GFP. Cell Metab. 2011 Dec 7;14(6):720–1.

16. Dixon BJ, Tang J, Zhang JH. The evolution of molecular hydrogen: a noteworthy potential therapy with clinical significance. Med Gas Res. 2013;3:10–10.

17. Tomanek L. Proteomic responses to environmentally induced oxidative stress. J Exp Biol. 2015;218(12):1867–1879.

18. Dauer W, Przedborski S. Parkinson's disease: mechanisms and models. Neuron. 39th ed. 2003;889–909.

19. Su KG, Banker G, Bourdette D, Forte M. Axonal degeneration in multiple sclerosis: The mitochondrial hypothesis. Curr Neurol Neurosci Rep. 2009 Sep;9(5):411–7.

20. Palau F, Estela A, Pla-Martín D, Sánchez-Piris M. The Role of Mitochondrial Network Dynamics in the Pathogenesis of Charcot-Marie-Tooth Disease. In: Espinós C, Felipo V, Palau F, editors. Inherited Neuromuscular Diseases: Translation from Pathomechanisms to Therapies [Internet]. Dordrecht: Springer Netherlands; 2009. p. 129–37.

21. Smith GM, Gallo G. The role of mitochondria in axon development and regeneration. Dev Neurobiol. 2017 Oct 14;78(3):221–37.

22. Chen H, Chan DC. Emerging functions of mammalian mitochondrial fusion and fission. Hum Mol Genet. 2005 Oct 15;14(suppl_2):R283–9.

23. Misko A, Jiang S, Wegorzewska I, Milbrandt J, Baloh RH. Mitofusin 2 is necessary for transport of axonal mitochondria and interacts with the Miro/Milton complex. J Neurosci Off J Soc Neurosci. 2010 Mar 24;30(12):4232–40.

24. Züchner S, Mersiyanova IV, Muglia M, Bissar-Tadmouri N, Rochelle J, Dadali EL, et al. Mutations in the mitochondrial GTPase mitofusin 2 cause Charcot-Marie-Tooth neuropathy type 2A. Nat Genet. 2004 Apr 4;36:449.

25. Cartoni R, Arnaud E, Médard J-J, Poirot O, Courvoisier DS, Chrast R, et al. Expression of mitofusin 2R94Q in a transgenic mouse leads to Charcot–Marie–Tooth neuropathy type 2A. Brain. 2010 May 1;133(5):1460–9.

26. Pich S, Bach D, Briones P, Liesa M, Camps M, Testar X, et al. The Charcot–Marie–Tooth type 2A gene product, Mfn2, up-regulates fuel oxidation through expression of OXPHOS system. Hum Mol Genet. 2005 Jun 1;14(11):1405–15.

27. Frohman EM, Racke MK, Raine CS. Multiple Sclerosis — The Plaque and Its Pathogenesis. N Engl J Med. 2006 Mar 2;354(9):942–55.

687 28. Sedel F, Bernard D, Mock DM, Tourbah A. Targeting demyelination and virtual hypoxia with
688 high-dose biotin as a treatment for progressive multiple sclerosis. Oligodendrocytes Health Dis.
689 2016 Nov 1;110:644–53.

690 29. Mahad DJ, Ziabreva I, Campbell G, Lax N, White K, Hanson PS, et al. Mitochondrial changes
691 within axons in multiple sclerosis. Brain J Neurol. 2009 May;132(Pt 5):1161–74.

692 30. Campbell G, Mahad DJ. Mitochondrial dysfunction and axon degeneration in progressive
693 multiple sclerosis. FEBS Lett. 2018 Feb 17;592(7):1113–21.

694 31. Gutscher M, Sobotta MC, Wabnitz GH, Ballikaya S, Meyer AJ, Samstag Y, et al. Proximity-based
695 Protein Thiol Oxidation by H(2)O(2)-scavenging Peroxidases. J Biol Chem. 2009 Nov
696 13;284(46):31532–40.

697 32. Imamura H, Huynh Nhat KP, Togawa H, Saito K, Iino R, Kato-Yamada Y, et al. Visualization of
698 ATP levels inside single living cells with fluorescence resonance energy transfer-based
699 genetically encoded indicators. Proc Natl Acad Sci U S A. 2009 Sep 15;106(37):15651–6.

700 33. Albrecht SC, Barata AG, Großhans J, Teleman AA, Dick TP. In Vivo Mapping of Hydrogen
701 Peroxide and Oxidized Glutathione Reveals Chemical and Regional Specificity of Redox
702 Homeostasis. Cell Metab. 2011 Dec 7;14(6):819–29.

703 34. Ren W, Ai H-W. Genetically Encoded Fluorescent Redox Probes. Sensors. 13th ed. 2013;15422–
704 33.

705 35. Tu H, Boppart SA. Coherent anti-Stokes Raman scattering microscopy: overcoming technical
706 barriers for clinical translation. J Biophotonics. 2014 Jan;7(0):9–22.

707 36. Mytskaniuk V, Bardin F, Boukhaddaoui H, Rigneault H, Tricaud N. Implementation of a Coherent
708 Anti-Stokes Raman Scattering (CARS) System on a Ti:Sapphire and OPO Laser Based Standard
709 Laser Scanning Microscope. J Vis Exp. 113th ed. 2016;doi: 10.3791/54262.

710 37. Hajjar H, Boukhaddaoui H, Rizgui A, Sar C, Berthelot J, Perrin-Tricaud C, et al. Label-free non-
711 linear microscopy to measure myelin outcome in a rodent model of Charcot-Marie-Tooth
712 diseases. J Biophotonics. 2018 Aug 9;0(ja):e201800186.

713 38. Huff TB, Cheng J-X. In vivo coherent anti-Stokes Raman scattering imaging of sciatic nerve
714 tissue. J Microsc. 2007 Feb;225(Pt 2):175–82.

715 39. Gonzalez S, Fernando R, Berthelot J, Perrin-Tricaud C, Sarzi E, Chrast R, et al. In vivo time-lapse
716 imaging of mitochondria in healthy and diseased peripheral myelin sheath. Mitochondrion.
717 2015 Jul 1;23:32–41.

718 40. Ino D, Sagara H, Suzuki J, Kanemaru K, Okubo Y, Iino M. Neuronal Regulation of Schwann Cell
719 Mitochondrial Ca2+ Signaling during Myelination. Cell Rep. 2015 Sep 29;12(12):1951–9.

720 41. Bernard-Marissal N, Van Hameren G, Juneja M, Pellegrino C, Rochat C, El Mansour O, et al.
721 Endoplasmic reticulum and mitochondria dysfunction underlies reversible Charcot–Marie–
722 Tooth type 2A neuropathy. (Under Review). under review;

723 42. Bazil JN, Beard DA, Vinnakota KC. Catalytic Coupling of Oxidative Phosphorylation, ATP
724 Demand, and Reactive Oxygen Species Generation. Biophys J. 2016 Feb 23;110(4):962–71.

725 43. Cadenas E, Davies KJA. Mitochondrial free radical generation, oxidative stress, and aging. Free
726 Radic Biol Med. 2000 Aug 1;29(3):222–30.

727 44. Bélanger E, Henry FP, Vallée R, Randolph MA, Kochevar IE, Winograd JM, et al. In vivo
728 evaluation of demyelination and remyelination in a nerve crush injury model. Biomed Opt
729 Express. 2011 Sep;2(9):2698–2708.

730 45. Cooper MF, Webster GR. The differentiation of phospholipase A1 and A2 in rat and human
731 nervous tissues. J Neurochem. 1970 Nov;17(11):1543–54.

732 46. Allt G, Ghabriel MN, Sikri K. Lysophosphatidyl choline-induced demyelination. Acta Neuropathol
733 (Berl). 1988 Sep 1;75(5):456–64.

734 47. Plemel JR, Michaels NJ, Weishaupt N, Caprariello AV, Keough MB, Rogers JA, et al. Mechanisms
735 of lysophosphatidylcholine-induced demyelination: A primary lipid disrupting myelinopathy.
736 Glia. 2017 Oct 25;66(2):327–47.

737 48. Kiryu-Seo S, Ohno N, Kidd GJ, Komuro H, Trapp BD. Demyelination increases axonal stationary
738 mitochondrial size and the speed of axonal mitochondrial transport. J Neurosci Off J Soc
739 Neurosci. 2010 May 12;30(19):6658–66.

740 49. Tricaud N, Park H. Wallerian demyelination: chronicle of a cellular cataclysm. Cell Mol Life Sci.
741 74th ed. 2017;4049–57.

742 50. Meiri H, Steinberg R, Medalion B. Detection of Sodium Channel Distribution in Rat Sciatic Nerve
743 Following Lysophosphatidylcholine-Induced Demyelination. J Membrane Biol. 92nd ed.
744 1986;47–56.

745 51. Hanson GT, Aggeler R, Oglesbee D, Cannon M, Capaldi RA, Tsien RY, et al. Investigating
746 Mitochondrial Redox Potential with Redox-sensitive Green Fluorescent Protein Indicators. J Biol
747 Chem. 2004 Mar 26;279(13):13044–53.

748 52. Dooley CT, Dore TM, Hanson GT, Jackson WC, Remington SJ, Tsien RY. Imaging Dynamic Redox
749 Changes in Mammalian Cells with Green Fluorescent Protein Indicators. J Biol Chem. 2004 May
750 21;279(21):22284–93.

751 53. Samara C, Poirot O, Domènech-Estévez E, Chrast R. Neuronal activity in the hub of
752 extrasynaptic Schwann cell-axon interactions. Front Cell Neurosci. 2013;7:228.

753 54. Yi M, Weaver D, Hajnóczky G. Control of mitochondrial motility and distribution by the calcium
754 signal: a homeostatic circuit. J Cell Biol. 2004 Nov 22;167(4):661–72.

755 55. Fukai T, Ushio-Fukai M. Superoxide Dismutases: Role in Redox Signaling, Vascular Function, and
756 Diseases. Antioxid Redox Signal. 2011 Sep 15;15(6):1583–606.

757 56. Yamakura F, Kawasaki H. Post-translational modifications of superoxide dismutase. Biochim
758 Biophys Acta. 1804th ed. 2010;318–25.

759 57. Little C, Olinescu R, Reid KG, O'Brien PJ. Properties and Regulation of Glutathione Peroxidase. J
760 Biol Chem. 1970 Jul 25;245(14):3632–6.

761 58. Nie Q, Wang C, Song G, Ma H, Kong D, Zhang X, et al. Mitofusin 2 deficiency leads to oxidative
762 stress that contributes to insulin resistance in rat skeletal muscle cells. Mol Biol Rep. 2014 Oct
763 1;41(10):6975–83.

764 59. Baloh RH, Schmidt RE, Pestronk A, Milbrandt J. Altered Axonal Mitochondrial Transport in the
765 Pathogenesis of Charcot-Marie-Tooth Disease from Mitofusin 2 Mutations. J Neurosci.
766 2007;27(2):422–430.

767 60. Zilberter Y, Zilberter T, Bregestovski P. Neuronal activity in vitro and the in vivo reality: the role
768 of energy homeostasis. Trends Pharmacol Sci. 2010 Sep 1;31(9):394–401.

769 61. Ainbinder A, Boncompagni S, Protasi F, Dirksen RT. Role of Mitofusin-2 in Mitochondrial
770 Localization and Calcium Uptake in Skeletal Muscle. Cell Calcium. 2015 Jan;57(1):14–24.

771 62. Chen Y, Csordás G, Jowdy C, Schneider TG, Csordás N, Wang W, et al. Mitofusin 2-containing
772 Mitochondrial-Reticular Microdomains Direct Rapid Cardiomyocyte Bioenergetic Responses via
773 Inter-Organelle Ca(2+) Crosstalk. Circ Res. 2012 Sep 14;111(7):863–75.

774 63. Yu T, Robotham JL, Yoon Y. Increased production of reactive oxygen species in hyperglycemic
775 conditions requires dynamic change of mitochondrial morphology. Proc Natl Acad Sci U S A.
776 2006 Feb 21;103(8):2653–8.

777 64. de Brito OM, Scorrano L. Mitofusin 2: A Mitochondria-Shaping Protein with Signaling Roles
778 Beyond Fusion. Antioxid Redox Signal. 2007 Dec 20;10(3):621–34.

779 65. Giorgio M, Migliaccio E, Orsini F, Paolucci D, Moroni M, Contursi C, et al. Electron Transfer
780 between Cytochrome c and p66Shc Generates Reactive Oxygen Species that Trigger
781 Mitochondrial Apoptosis. Cell. 2005 Jul 29;122(2):221–33.

782 66. Chen H, Chan DC. Mitochondrial dynamics–fusion, fission, movement, and mitophagy–in
783 neurodegenerative diseases. Hum Mol Genet. 2009 Oct 15;18(R2):R169–76.

784 67. Bros H, Millward JM, Paul F, Niesner R, Infante-Duarte C. Oxidative damage to mitochondria at
785 the nodes of Ranvier precedes axon degeneration in ex vivo transected axons. Exp Neurol. 2014
786 Nov 1;261:127–35.

787 68. Witte ME, Bø L, Rodenburg RJ, Belien JA, Musters R, Hazes T, et al. Enhanced number and
788 activity of mitochondria in multiple sclerosis lesions. J Pathol. 2009 May 26;219(2):193–204.

789 69. Young EA, Fowler CD, Kidd GJ, Chang A, Rudick R, Fisher E, et al. Imaging correlates of
790 decreased axonal Na+/K+ ATPase in chronic multiple sclerosis lesions. Ann Neurol.
791 2008;63(4):428–35.

792 70. Gilgun-Sherki Y, Melamed E, Offen D. The role of oxidative stress in thepathogenesis of multiple
793 sclerosis: The need for effectiveantioxidant therapy. J Neurol. 2004 Mar 1;251(3):261–8.

794 71. Rousset S, Alves-Guerra M-C, Mozo J, Miroux B, Cassard-Doulcier A-M, Bouillaud F, et al. The
795 Biology of Mitochondrial Uncoupling Proteins. Diabetes. 2004;53(suppl 1):S130–S135.

796 72. Dalgaard LT, Pedersen O. Uncoupling proteins: functional characteristics and role in the
797 pathogenesis of obesity and Type II diabetes. Diabetologia. 2001 Aug 1;44(8):946–65.

798 73. Rexroth S, Poetsch A, Rögner M, Hamann A, Werner A, Osiewacz HD, et al. Reactive oxygen
799 species target specific tryptophan site in the mitochondrial ATP synthase. Biochim Biophys Acta
800 BBA - Bioenerg. 2012 Feb 1;1817(2):381–7.

801 74. Yin X, Kidd GJ, Ohno N, Perkins GA, Ellisman MH, Bastian C, et al. Proteolipid protein–deficient
802 myelin promotes axonal mitochondrial dysfunction via altered metabolic coupling. J Cell Biol.
803 2016 Nov 21;215(4):531–42.

804 75. Yellen G. Fueling thought: Management of glycolysis and oxidative phosphorylation in neuronal
805 metabolism. J Cell Biol. 2018;217(7):2235–2246.

806 76. Funfschilling U, Supplie LM, Mahad D, Boretius S, Saab AS, Edgar J, et al. Glycolytic
807 oligodendrocytes maintain myelin and long-term axonal integrity. Nature. 2012 Apr
808 29;485(7399):517–21.

809 77. Stefanini M, Martino CD, Zamboni L. Fixation of Ejaculated Spermatozoa for Electron
810 Microscopy. Nature. 1967 Oct 14;216:173.

811 78. Hung H, Kohnken R, Svaren J. The NURD chromatin remodeling complex is required for
812 peripheral nerve myelination. J Neurosci. 2012 Feb 1;32(5):1517–27.